First- and second-order piezoelectricity in III-V semiconductors

Annie Beya-Wakata, Pierre-Yves Prodhomme, and Gabriel Bester*
Max-Planck-Institut für Festkörperforschung, Heisenbergstrasse 1, DE-70569 Stuttgart, Germany
(Received 6 June 2011; revised manuscript received 3 November 2011; published 28 November 2011)

We present the results of first-principles plane-wave pseudopotential calculations of piezoelectric coefficients of first and second order for a total of nine III-V binary phases (AlP, AlAs, AlSb, GaP, GaAs, GaSb, InP, InAs, InSb) of zinc-blende semiconductors. These coefficients are used to calculate the piezoelectric fields for [111]-oriented quantum wells (QWs) with different well-barrier combinations and various dimensions. We derive an approximate analytic expression for the strain tensor in the case of pseudomorphic growth along an arbitrary growth direction. Together with the piezoelectric coefficients, this allows a simple calculation of the piezoelectric field up to second order in strain for an arbitrary growth direction and any material combination within the nine III-Vs presented here. Nonlinear contributions to the polarization are shown to be of significant magnitude for all the materials presented. In some cases the field is increased by the second-order terms; in some cases it is decreased. We analyze the chemical trends of the obtained coefficients. We compare our results to available experiments and find good agreement in one-third of the cases, while for the remaining cases the calculated field is larger to significantly larger than in the measurements. We discuss the popular experimental techniques and highlight possible reasons for the discrepancies.

DOI: 10.1103/PhysRevB.84.195207 PACS number(s): 77.65.Bn, 73.21.Fg, 77.65.Ly

I. INTRODUCTION

Heterostructures, made of materials with different lattice constants, are subjected to elastic deformations. In the presence of a shear strain, piezoelectric fields develop in crystals with zinc-blende structure. The existence of internal piezoelectric fields (sign, magnitude, as well as their consequences) within [111]-grown strained semiconductor layers was established theoretically in a series of papers by Mailhiot and Smith.[1–7] In fact, the [111] orientation offers the possibility to produce piezoelectric fields, which can easily exceed 100 kV/cm. Since then, a great deal of theoretical and experimental research has been devoted to the understanding of the piezoelectric properties of bulk (e.g., Refs. 8 and 9), quantum wells (QWs) (e.g., Refs. 10–12), quantum wires (e.g., Refs. 13–15), and quantum dots (e.g., Refs. 16–20). The work on QWs has been especially decisive since the screening of the piezoelectric fields can be strongly reduced under most experimental conditions. Conclusions drawn from bulk measurements, on the other hand, are usually shadowed by the appearance of free carriers (residual, intrinsic, or photoinduced) effectively screening the field. In the case of III-V zinc-blende heterostructures specifically, the intrinsic strain-induced electric fields are held responsible for strong effects on the transport properties,[21] optical characteristics,[22–24] and acousto-optical modulation[25] in a way which may lead to the microstructural engineering of novel optical and electronic devices.[26,27] The interest on these modified properties is therefore manyfold: the understanding of the physics involved and the development of new applications, that is, integrated, mixed-effect devices, optical switches, modulators, and nonlinear devices.[28–32] A recent paper by Lew Yan Voon[33] reviews recent work involving piezoelectric effects.

The existence of a nonlinear piezoelectric effect, subject to this work, was first mentioned by Cibert *et al.*[34,35] for II-VI CdTe QWs. They argued that this material was an ideal candidate for nonlinear piezoelectric effects due to its small piezoelectric coefficient. They measured a piezoelectric field that depended in a nonlinear fashion on the elastic strain. Subsequent theoretical calculations[36] showed that the piezoelectric tensor in CdTe strongly depends on the hydrostatic pressure, but very little on the traceless strain. The author concluded that for CdTe, where the linear coefficient is very small, its hydrostatic strain dependence should be taken into account. They further speculated that the nonlinear terms should give a small contribution in materials such as GaAs, due to a large linear piezoelectric effect. The methodology for the calculation of second-order piezoelectricity within density functional theory was developed by Bester *et al.*[37] and applied to the III-V InAs/GaAs QWs.[37] The effect of the second-order terms for $In_xGa_{1-x}As$/GaAs [111] QWs with conventional compositions ($x \leqslant 0.20$) was shown to reduce the field by around 20%. In the case of the popular $In_xGa_{1-x}As$ quantum dots embedded in GaAs, the second-order effect was shown to nearly cancel the first-order effect.[38] The investigation on the balance between linear and quadratic piezoelectric terms was then extended to QDs of different shapes and compositions.[13,18,19,39,40] The effect of second-order piezoelectricity on the pressure coefficient of the light emission was further investigated in InGaAs/GaAs QWs.[41] The calculations revealed that changes of the built-in electric field with pressure in (111)-oriented QWs are significantly enlarged by the effect of nonlinear piezoelectricity, in comparison to the case when linear piezoelectricity is used.[41]

In this paper we calculate via first-principles plane-wave pseudopotentials calculations the linear and quadratic piezoelectric coefficients for a total of nine III-V binary compounds ([Al,Ga,In]-[P,As,Sb]) with zinc-blende structure. Using these coefficients we calculate the piezoelectric fields for 14 different QWs. We find large nonlinear contributions for all the investigated materials. The paper is organized as follows. In Sec. II we review the methodology and outline the computational details. We present our results and discuss trends we can identify in the obtained coefficients. Section III presents the methods used for the calculation of the piezoelectric fields from the piezoelectric coefficients. First, some considerations from electrostatics are

presented. Then, the special case of a [111] QW is illustrated, as is the procedure to obtain the polarizations and fields for arbitrary crystallographic directions. Section IV describes the electric fields we obtained for 14 different QWs grown along the [111] direction. Section V focuses on the InGaAs/GaAs material system but shows results for arbitrary crystallographic growth direction. In Sec. VI we discuss the experimental techniques used to extract piezoelectric fields and in Sec. VII we compare our results to experiment. In Sec. VIII we point out the importance of QW and barrier thicknesses, as well as QW composition.

II. CALCULATION OF PIEZOELECTRIC COEFFICIENTS UP TO SECOND ORDER IN STRAIN

A. Methodology

Piezoelectricity is defined as the generation of electric polarization by application of stress to a crystal lacking a center of inversion. The electric polarization P_μ as a function of mechanical strain $\eta_{\alpha\beta}$ can be written assuming summation over repeating index and retaining the second order in strain as

$$P_\mu = \sum_{\alpha\beta} e_{\mu\alpha\beta}\eta_{\alpha\beta} + \frac{1}{2}\sum_{\alpha\beta\gamma\lambda} B_{\mu\alpha\beta\gamma\lambda}\eta_{\alpha\beta}\eta_{\gamma\lambda}, \tag{1}$$

where $e_{\mu\alpha\beta}$ is the third-rank proper piezoelectric tensor of the unstrained material, while $B_{\mu\alpha\beta\gamma\lambda}$ is a fifth-rank tensor defined below. The Greek indexes μ, α, β, γ, and λ stand for the x, y, and z axes of the Cartesian coordinate system. The six independent components of the strain tensor are given in the Voigt notation as

$$\eta_1 = \eta_{xx}, \quad \eta_2 = \eta_{yy}, \quad \eta_3 = \eta_{zz},$$
$$\eta_4 = 2\eta_{yz}, \quad \eta_5 = 2\eta_{xz}, \quad \eta_6 = 2\eta_{xy}.$$

We use Latin letters $(i,j,k,\ldots)$ for the Voigt index. Note that some authors, for example, Grimmer,[42] do not use the factor of 1/2 in Eq. (1), which simply results in a different definition of B. The polarization component can then be written as

$$P_\mu = \sum_{j=1}^{6} e_{\mu j}\eta_j + \frac{1}{2}\sum_{jk=1}^{6} B_{\mu jk}\eta_j\eta_k, \tag{2}$$

where $B_{\mu jk}$ represents the first-order change of the piezoelectric tensor with strain. Following this definition, the piezoelectric tensor can be defined as a function of strain

$$\tilde{e}_{\mu j}(\eta) = \frac{dP_\mu}{d\eta_j} = e_{\mu j} + \sum_k B_{\mu jk}\eta_k. \tag{3}$$

The tensor $B_{\mu\alpha\beta\gamma\lambda}$ is symmetric under an interchange of $\alpha\beta$ and $\gamma\lambda$. It follows that $B_{\mu jk}$ is symmetric under an interchange of j and k. The form of the fifth-rank piezoelectric tensor for the 21 noncentrosymmetric crystallographic point groups was first determined by Koptsik and later by Nelson in a particular orientation.[43,44] Recently, Grimmer[42] derived the form of the second-order piezoelectric tensor for crystals and quasicrystals of any symmetry and for all the orientations. The orientation of the symmetry elements for the zinc-blende crystal structure [T_d, $F(\bar{4}3m)$] show that there are three nonzero coefficients for $e_{\mu j}$ and that there is only one independent element to be determined: $e_{14} = e_{25} = e_{36}$. The symmetry restrictions on the $B_{\mu jk}$ tensor lead to 24 nonzero coefficients with only three independent ones:

$$B_{114} = B_{225} = B_{336},$$
$$B_{124} = B_{235} = B_{316} = B_{134} = B_{215} = B_{326},$$
$$B_{156} = B_{345} = B_{246}.$$

The relations for the linear and quadratic dependence of the polarization on the strain tensor are given by $\boldsymbol{P} = \boldsymbol{P}_l + \boldsymbol{P}_{nl}$, with

$$\boldsymbol{P}_l = e_{14}\begin{pmatrix}\eta_4\\ \eta_5\\ \eta_6\end{pmatrix},$$

$$\boldsymbol{P}_{nl} = B_{114}\begin{pmatrix}\eta_1\eta_4\\ \eta_2\eta_5\\ \eta_3\eta_6\end{pmatrix} + B_{124}\begin{pmatrix}\eta_4(\eta_2+\eta_3)\\ \eta_5(\eta_3+\eta_1)\\ \eta_6(\eta_1+\eta_2)\end{pmatrix} + B_{156}\begin{pmatrix}\eta_5\eta_6\\ \eta_4\eta_6\\ \eta_4\eta_5\end{pmatrix}. \tag{4}$$

Our calculations of these tensor elements rely on the density functional perturbation theory (DFPT) techniques applied in the local density approximation (LDA) and the generalized gradient approximation (GGA) for the exchange correlation functional. The results reported here were obtained from an implementation of the LDA in the framework of the ABINIT code package.[45] The calculations were carried out using the Troullier-Martins (TM) pseudopotentials,[46] prepared by the Fritz Haber Institute code.[47] Some calculations were also done using the relativistic separable pseudopotentials in the form of Hartwigsen, Goedecker, and Hutter (HGH).[48] The numerical results presented were computed by treating the electrons of the $3d$ (Ga) and $4d$ (In) level as valence states. Plane waves up to 100 Ha were used to expand the electronic states and the Brillouin zone was sampled with a mesh of $12 \times 12 \times 12$ k points.

In order to obtain the coefficients $e_{\mu j}$ and $B_{\mu jk}$ we proceeded in the following manner. First, we relaxed the lattice parameters for the binary compounds [Al, Ga, In]-[P, As, Sb]. Next, linear-response calculations of the linear bulk piezoelectric constant $e_{\mu j}$ were carried out on these relaxed structures using the DFPT module of the ABINIT package,[49,50] which implements a direct calculation of the strain derivatives of the quantities of interest (Kohn-Sham wavefunctions, polarizations, etc.) via a chain rule. Then, a finite-difference technique was used in order to obtain the "improper" (see next section) nonlinear bulk piezoelectric tensors $B^i_{\mu jk}$. With the strain η_i frozen at a particular value δ, the ions were allowed to relax, after which the piezoelectric tensor elements $\tilde{e}_{\mu j}(\delta)$ were computed using linear-response techniques. This is repeated for several values of δ up to 2% for the diagonal elements and up to 0.2% for the nondiagonal elements, then the dependence of these elements on δ is fitted, and the linear dependence extracted. This was done for different strains η_i leading, in a first step, to different improper second-order coefficients $B^i_{\mu jk}$.

B. From improper to proper second-order coefficients

Until now, except for the last paragraph, we implicitly talked about the "proper" coefficients. It has already been shown that the proper (linear) piezoelectric coefficient e^p does

not depend on the branch of the polarization as the improper piezoelectric coefficient e^i does.[51] We emphasize here that a naive computation of the second-order coefficient leads to an improper coefficient and that it needs to be corrected in order to get the proper second-order coefficient. The proper coefficients should be directly comparable to the experimental one; that is, they should not depend on the branch of polarization.

In order to derive the proper second-order piezoelectric tensor we use Cartesian coordinates, instead of the Voigt index:

$$B^i_{\mu\alpha\beta\gamma\lambda} = \frac{d\tilde{e}^p_{\mu\alpha\beta}}{d\eta_{\gamma\lambda}}. \tag{5}$$

According to Vanderbilt,[51] the proper piezoelectric tensor is given by

$$\tilde{e}^p_{\mu\alpha\beta} = -\frac{1}{2\pi}\frac{q}{\Omega}\sum_\nu \frac{d\phi_\nu}{d\eta_{\alpha\beta}}\mathbf{R}_{\nu\mu}, \tag{6}$$

with ϕ_ν the total Berry phase in direction ν, Ω the volume of the unit cell, and q the electronic charge. So the improper second-order piezo coefficient is given by

$$B^i_{\mu\alpha\beta\gamma\lambda} = \frac{1}{2\pi}\frac{q}{\Omega^2}\frac{d\Omega}{d\eta_{\gamma\lambda}}\sum_\nu \frac{d\phi_\nu}{d\eta_{\alpha\beta}}\mathbf{R}_{\nu\mu} - \frac{1}{2\pi}\frac{q}{\Omega}\sum_\nu \frac{d\phi_\nu}{d\eta_{\alpha\beta}}\frac{d\mathbf{R}_{\nu\mu}}{d\eta_{\gamma\lambda}} - \frac{1}{2\pi}\frac{q}{\Omega}\sum_\nu \frac{d^2\phi_\nu}{d\epsilon_{\alpha\beta}d\epsilon_{\gamma\lambda}}\mathbf{R}_{\nu\mu}. \tag{7}$$

Then one has to remember the definition of a strained vector and a strained volume,

$$\mathbf{R}_{\nu\alpha} = \mathbf{R}^0_{\nu\alpha} + \sum_\tau \eta_{\nu\tau}\mathbf{R}^0_{\tau\alpha}, \tag{8}$$

and

$$\Omega = \Omega_0 + \sum_\tau \eta_{\tau\tau}\Omega_0. \tag{9}$$

Since by definition the strain is symmetric (otherwise it is a strain + rotation), the following property has to be ensured:

$$\eta_{\nu\tau} = \eta_{\tau\nu} = \tfrac{1}{2}(\eta_{\nu\tau} + \eta_{\tau\nu}). \tag{10}$$

This is an important point since otherwise the B's can lack symmetry. Applying this property to the derivatives of the real space lattice vectors and in the volume derivatives one finds

$$\frac{d\mathbf{R}_{\nu\alpha}}{\eta_{\gamma\lambda}} = \frac{1}{2}\sum_\tau(\delta_{\nu\gamma}\delta_{\tau\lambda} + \delta_{\nu\lambda}\delta_{\tau\gamma})\mathbf{R}^0_{\tau\alpha}, \tag{11}$$

and

$$\frac{d\Omega}{d\eta_{\gamma\lambda}} = \sum_\tau \delta_{\tau\gamma}\delta_{\tau\lambda}\Omega_0. \tag{12}$$

Thus, one finds (remembering that the piezoelectric coefficients are calculated at zero strain, that is, $\mathbf{R} = \mathbf{R}^0$ and $\Omega = \Omega_0$),

$$B^i_{\mu\alpha\beta\gamma\lambda} = \frac{1}{2\pi}\frac{q}{\Omega}\delta_{\gamma\lambda}\sum_\nu \frac{d\phi_\nu}{d\eta_{\alpha\beta}}\mathbf{R}_{\nu\mu} - \frac{1}{2\pi}\frac{q}{\Omega}\sum_\nu \frac{d\phi_\nu}{d\eta_{\alpha\beta}} \times \frac{1}{2}(\delta_{\mu\gamma}\mathbf{R}_{\nu\lambda} + \delta_{\mu\lambda}\mathbf{R}_{\nu\gamma}) - \frac{1}{2\pi}\frac{q}{\Omega}\sum_\nu \frac{d^2\phi_\nu}{d\eta_{\alpha\beta}d\eta_{\gamma\lambda}}\mathbf{R}_{\nu\mu}. \tag{13}$$

The last term is what we call the proper second-order piezoelectric coefficient $B^p_{\mu\alpha\beta\gamma\lambda}$.

Rearranging the terms, one finally gets

$$B^p_{\mu\alpha\beta\gamma\lambda} = B^i_{\mu\alpha\beta\gamma\lambda} + \delta_{\gamma\lambda}e_{\mu\alpha\beta} - \tfrac{1}{2}(\delta_{\mu\gamma}e_{\lambda\alpha\gamma} + \delta_{\mu\lambda}e_{\gamma\alpha\beta}). \tag{14}$$

Explicitly, the second-order piezoelectric coefficients calculated in this work are [when the B's have three (five) indices it represents the Voigt (Cartesian) notation]

$$\begin{aligned}
B^p_{114} &= B^p_{11123} = B^i_{11123} + \delta_{23}e_{111} - \tfrac{1}{2}(\delta_{12}e_{311} + \delta_{13}e_{211}),\\
B^p_{114} &= B^i_{114},\\
B^p_{141} &= B^p_{12311} = B^i_{12311} + \delta_{11}e_{123} - \tfrac{1}{2}(\delta_{11}e_{123} + \delta_{11}e_{123}),\\
B^p_{141} &= B^i_{141},\\
B^p_{124} &= B^p_{12223} = B^i_{12223} + \delta_{23}e_{122} - \tfrac{1}{2}(\delta_{12}e_{222} + \delta_{13}e_{222}),\\
B^p_{124} &= B^i_{124},\\
B^p_{142} &= B^p_{12322} = B^i_{12322} + \delta_{22}e_{123} - \tfrac{1}{2}(\delta_{12}e_{223} + \delta_{12}e_{223}),\\
B^p_{142} &= B^i_{142} + e_{14},\\
B^p_{156} &= B^p_{11312} = B^i_{11312} + \delta_{12}e_{113} - \tfrac{1}{2}(\delta_{11}e_{213} + \delta_{12}e_{113}),\\
B^p_{156} &= B^i_{156} - \tfrac{1}{2}e_{25},\\
B^p_{165} &= B^p_{11213} = B^i_{11213} + \delta_{13}e_{112} - \tfrac{1}{2}(\delta_{11}e_{312} + \delta_{13}e_{112}),\\
B^p_{165} &= B^i_{165} - \tfrac{1}{2}e_{36}.
\end{aligned}$$

To illustrate quantitatively this correction, we take the coefficients B_{124} and B_{142} of GaAs. The straightforward calculation described in Sec. II A leads to the improper coefficients, -3.78 C/m^2 and -3.54 C/m^2, respectively. Applying the correction, we find that the corresponding proper coefficients are equal and amount to -3.78 C/m^2. The correction therefore restores a fundamental symmetry of the coefficients. In this case, the proper B_{142} and B_{124} deviate by less than 0.01 C/m^2, which is below the precision we expect from the convergence of the parameters (0.05 C/m^2).

Here we should add that the proper second-order piezoelectric tensor could be calculated more straightforwardly by using the second derivative of the energy. One should first calculate the reduced second-order tensor by finite difference:

$$B^r_{\nu ij} = \frac{\delta}{\delta\eta_j}\left[\frac{d^2E_c}{d\eta_i d\epsilon_\nu} + \frac{d^2E_c}{ds_{\tau\mu}d\eta_i}\left(\frac{d^2E_c}{ds_{\alpha\beta}ds_{\gamma\lambda}}\right)^{-1}_{\tau\mu\tau'\mu'}\frac{d^2E_c}{ds_{\tau'\mu'}d\epsilon_\nu}\right], \tag{15}$$

with ϵ_ν the reduced electric field in direction ν, $s_{\alpha\beta}$ the small displacement of ions with α and β running on each atom in all three directions of the unit cell vectors, and E_c the energy of the unit cell. Then one should be able to compute the proper second-order piezoelectric coefficient as

$$B^p_{\alpha ij} = -\frac{q}{\Omega_0}B^r_{\nu ij}\mathbf{R}_{\nu\alpha}. \tag{16}$$

We underline here that in what follows we only consider the proper piezoelectric tensor.

TABLE I. Linear and quadratic piezoelectric coefficients (C/m^2) as calculated from LDA-DFT. We report the lattice constant (bohr) at which the calculation has been done. The materials accompanied with an asterisk are uncertain, and the uncertainty is put into square brackets if above our 0.05 C/m^2 precision.

	e_{14}	B_{114}	B_{124}	B_{156}	a_0	a_0^{exp}	e_{14}^{exp}
AlP	−0.033	−1.9	−2.7	−1.3	10.222	10.301	Unknown
AlAs	−0.048	−1.5	−2.6	−1.2	10.619	10.699	Unknown
AlSb	−0.084	−0.7	−2.2	−0.7	11.478	11.594	0.157, 0.068
GaP	−0.131	−0.7	−3.6	−0.9	10.235	10.273	−0.15
GaAs	−0.238	−0.4	−3.8	−0.7	10.645	10.683	−0.16
GaSb*	−0.247	0.2 [±0.1]	−3.2 [±0.1]	0.0	11.378	11.519	−0.12
InP	0.003	−1.1	−3.8	−0.5	11.042	11.090	Unknown
InAs*	−0.115	−0.6 [±0.1]	−4.1	0.2	11.432	11.449	−0.045, −0.12
InSb*	−0.159	0.1	−3.5	0.6	12.141	12.243	−0.071, −0.097

C. Reduction of the number of calculation and consistency checks based on symmetry considerations

The step-by-step methodology used to calculate the second order piezoelectric coefficients was described in Sec. II A. However, it is convenient to calculate the coefficients of interest by noticing the specific symmetry of the second-order tensor (presented in Sec. II A). By considering a [111] shear strain $\eta = (0,0,0,\delta,\delta,\delta)$ in Eq. (3), one is able to obtain in one calculation $\tilde{e}_{11}(\delta) = \tilde{e}_{11}(\eta_4)$, $\tilde{e}_{12}(\delta) = \tilde{e}_{12}(\eta_5)$, and $\tilde{e}_{15}(\delta) = \tilde{e}_{15}(\eta_6)$, which gives, after correction, the proper coefficient B_{114}, B_{124}, B_{156}.

However, applying different deformations to obtain one second-order coefficient serves as a consistency check. For instance, the relation

$$B_{141} = B_{114} \tag{17}$$

must hold and can be checked by calculating the η_1 dependence of e_{14} and the η_4 dependence of e_{11}. In this case, no correction is required and the linear slopes of these dependences give the proper second-order coefficients, and they must be equal. So with only few calculations with hydrostatic and uniaxial strains, it is possible to calculate the three nonlinear coefficients and check them.

D. Results

The numerical values of the first- and second-order piezoelectric coefficients are given in Table I along with the lattice constant (in Bohr) at which the calculations were performed. The materials with zero band gap in the calculations are marked with an asterisk and the error bars are given in square brackets. In the last two columns, the experimental values of the lattice constant and the linear piezoelectric constant are reported. A graphical representation of these results is given in Fig. 1. The nine semiconductors are arranged according to the Periodic Table on a grid and the height of the columns is given by the negative value of the coefficients. The colors are distributed for each panel (coefficient) from blue to red according to the magnitude of the coefficients, blue being attributed to the smallest. We can see large variations within the nine III-V's in the value of the coefficients for e_{14}, B_{114}, and B_{156} with even some changes in sign. In contrast, the magnitudes of B_{124} are large and rather constant for the nine materials. All four coefficients seem to underlie a different trend: For e_{14} the coefficients become larger along the series phosphide → arsenide → antimonide. There is no recognizable trend along Al → Ga → In. The magnitude of e_{14} is largest for the Ga compounds. For B_{114} the trend seems reversed and the coefficients go from large to small (even from positive to negative for the In and Ga compounds) in the direction Sb → As → P. For B_{124} the trend follows Al → Ga → In with increasing magnitudes; qualitatively different than the trends for e_{14} and B_{114}. The trend for B_{156} is yet another one and goes across the series, going from a positive coefficient for InSb (0.6) to a negative one for AlP (−1.3), seemingly following the mass or the lattice constant of the compound. To highlight this trend we plotted in Fig. 2 the piezoelectric coefficients as a function of the compound's

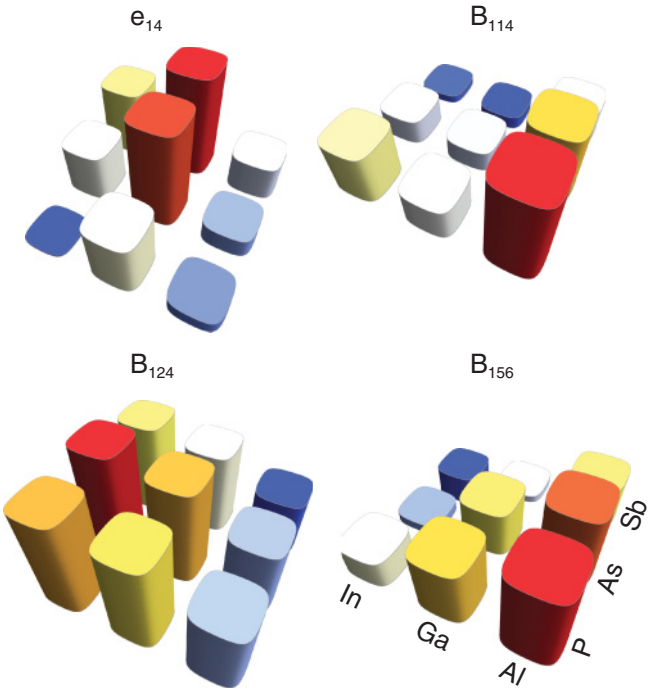

FIG. 1. (Color online) Graphical display of the piezoelectric coefficients. The height of the columns (also indicated by the color code, from blue to red) give the negative values of the coefficients.

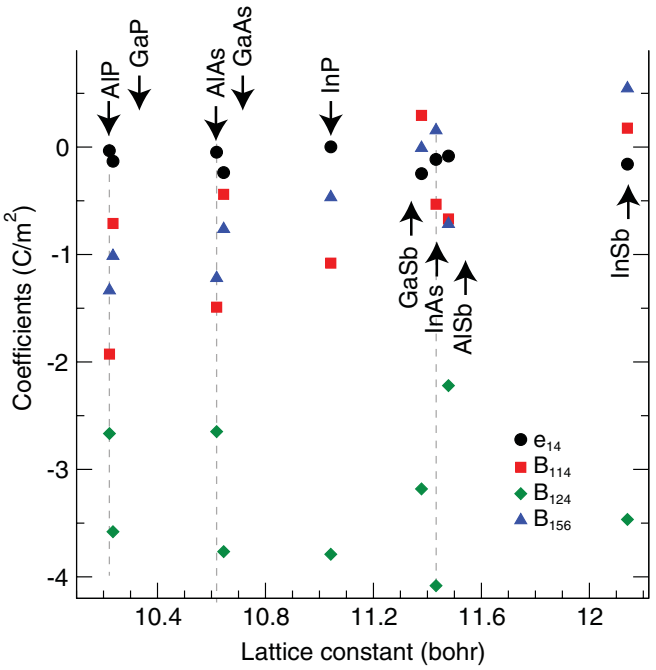

FIG. 2. (Color online) Piezoelectric coefficients as a function of the lattice constants.

lattice constants. A relatively clear trend with lattice constant can be only observed for B_{156} as just noted.

As for the importance of the second-order coefficients we present calculations on QWs made of the different materials. However, from the coefficients alone, we can anticipate that for materials with very small e_{14} and large second-order coefficients, such as the aluminides and InP, the nonlinear effects will dominate the piezoelectric properties.

To gauge the effect of the chosen exchange correlation function, we performed additional calculations using the GGA. The results are given in Table II. We see that the value of the B's for LDA and GGA are comparable, while the values of e_{14} are quite different. This difference is attributed to the values used for the lattice constant in both approximations. The GGA leads for GaAs and InAs to lattice constants significantly larger than the experimental values so that we assess the LDA values as more accurate. In general, the calculated lattice constants reported in Table I are in good agreement with experiment.

We also note significant discrepancies with previously calculated B_{156} coefficients[37] for InAs and GaAs. For GaAs, our present value (-0.763 C/m^2) is around 50% larger in magnitude than the earlier value (-0.492 C/m^2[37]) and for InAs even the sign is opposite (0.156 here vs -0.120 earlier[37]).

TABLE II. Linear and quadratic piezoelectric coefficients (C/m^2) as calculated from GGA-DFT. The lattice constant (bohr) at which the calculation has been done is reported in the last column and is significantly larger than reported experimentally. We discard these results as less accurate.

	e_{14}	B_{114}	B_{124}	B_{156}	a_0
GaAs	-0.342	-0.5	-4.1	-0.6	10.948
InAs	-0.241	-0.5	-4.4	0.1	11.764

The facts that the remaining coefficients are in excellent agreement with this previous work[37] and that we do not see fluctuations of nearly that magnitude by using different levels of approximation (pseudopotentials used and exchange correlation functional), leads us to believe that the previous results must have been erroneous. A negative B_{156} coefficient for InAs was obtained independently.[52]

E. Accuracy of the results and issues with zero-gap materials

Overall, the electronic structure parameters (number of k points, energy cutoff) were chosen to reach an accuracy of 0.05 C/m^2 on the B's.

However, since DFT (LDA or GGA) is well known to estimate roughly the electronic band dispersion, and in particular it underestimates the band gap, it happens in our calculations that for some materials with small gap (GaSb, InAs, InSb) the gap was found to be null. For those materials, despite all the care we took to ensure convergence (k points, cutoff, relaxation, etc.), we obtain discrepancies between coefficients that must be identical on symmetry grounds (under Voigt indices interchange). We interpret these discrepancies as arising from the self-consistent change of the density, in response to the applied strain, that can be affected by the pathological situation of vanishing band gaps. For example, for the GaSb compound, we find $B_{114} = 0.30$ C/m^2 and $B_{141} = 0.18$ C/m^2, although these should be equal. So for this material we retain only the average value and we consider the error as the difference between the two values; this is ± 0.12 C/m^2. This value is given as error bars in our final results. For these materials, we also have reasons to doubt the accuracy of the linear coefficients. Using pseudopotentials without d states opens the band gap and changes the results for e_{14} quite dramatically (for InAs, the coefficient changes from -0.115 to $+0.066$ C/m^2) while this change is smaller for materials with nonzero band gap at the LDA level. These changes are tied with the strong dependence on the lattice constant (that is just given by the B's) and it is difficult to estimate an error bar. Our impression, however, is that the linear coefficients for materials with zero gap in LDA/GGA may be improved by methods yielding a proper band gap (e.g., GW), not available at the moment.

F. Harrison model of piezoelectricity

Here we give a short introduction to the popular Harrison model of piezoelectricity which gives an intuitive picture of piezoelectricity. Harrison[53] followed the idea of the bond-orbital model.[54] He defined the microscopic electric dipole of a pair of anion-cation induced by a lattice deformation η_4 as the piezoelectric dipole p:

$$p = \delta d\, e_P^* e \quad \text{with} \quad \delta d = \xi \eta_4 a/8, \tag{18}$$

with a the lattice constant, e_P^* the so-called piezoelectric charge, and e the electron charge. The internal displacement of the metallic relative to the nonmetallic atom is given by δd. Without any change in the physics it is rewritten for a zinc-blende structure using the Kleinman parameter ξ. The piezoelectric charge e_P^* is also commonly rewritten using

parameters from the bond-orbital model as

$$e_P^* = Z^* - \frac{8\alpha_p\left(1-\alpha_p^2\right)(1-\xi)}{3\xi}, \tag{19}$$

where Z^* is the effective charge of the material and α_p the polarity of the bond, both originally defined based on a linear combination of atomic orbitals model.[54] Since Z^* can be directly related to α_p[54] this model of piezoelectricity requires only two parameters, namely, ξ and α_p. While these parameters have an intuitive meaning, they cannot be measured or calculated directly. They are usually extracted from some experimental quantities and can then be reused to predict other quantities. In the original work of Harrison[53] the calculated piezoelectric charge e_P^* was in poor agreement with the values deduced from experimental piezoelectric constants. However, this is not surprising since the piezoelectric response is a delicate balance between a *clamped-ion* part and an *internal-strain* part[55] that depend sensitively on the chosen parameter. Indeed, an adjustment of the parameters brings experiment and theory in agreement (at the expense to bring about a disagreement with the experiment from which the parameters were extracted from originally). The benefit of the model lies in its simplicity and the intuitive picture it draws. The generality of Eq. (18) makes it possible to introduce strain dependence beyond the trivial linear term in δd. This has been recently done by Migliorato *et al.*[56] for $In_xGa_{1-x}As$. In this work, the bond polarity α_p was taken from a tight-binding model and the Kleinman parameters were calculated by DFT. The effective charges Z^* of InAs and GaAs were not calculated from α_p[54] but were used as fitting parameters to reproduce the experimentally determined piezoelectric coefficients of bulk InAs and GaAs. Using the same strain dependence for α_p and Z^* and a linear interpolation between different compositions, the piezoelectric charge and hence coefficient, show a bowing toward less negative values, compared to a treatment linear in strain. This bowing is in agreement with our *ab initio* results where the second-order terms make the effective piezoelectric coefficient less negative.

III. CALCULATION OF PIEZOELECTRIC FIELDS IN QUANTUM WELLS

A. Considerations from electrostatics

From the electrostatic equations of dielectrics the displacement field $\boldsymbol{D}$ is introduced as

$$\boldsymbol{D} = \varepsilon_0 \boldsymbol{E} + \boldsymbol{P}, \tag{20}$$

with the electronic polarization $\boldsymbol{P}$ describing the electronic response to the applied external field $\boldsymbol{E}$. Using the permittivity tensor,

$$\boldsymbol{\varepsilon} \equiv \varepsilon_{\alpha\beta} = \frac{1}{\varepsilon_0}\frac{\partial \boldsymbol{D}_\alpha}{\partial \boldsymbol{E}_\beta}, \tag{21}$$

we obtain

$$\boldsymbol{P} = \varepsilon_0(\boldsymbol{\varepsilon} - 1)\boldsymbol{E} + \boldsymbol{P}_0, \tag{22}$$

where $\boldsymbol{P}_0$ and ε_0 are the zero-electric-field polarization and the permittivity of the vacuum, respectively. Assuming a linear relation between the applied electric field and the ensuing electronic polarization and an isotropic medium, we can rewrite it

$$\boldsymbol{P} = \varepsilon_0 \boldsymbol{\chi}_e \boldsymbol{E} + \boldsymbol{P}_0, \tag{23}$$

using the electrical susceptibility tensor $\boldsymbol{\chi}_e = \boldsymbol{\varepsilon} - 1$. The polarization $\boldsymbol{P}_0$ can only be nonzero if the medium lacks inversion symmetry. In the case of a piezoelectric material this is the case and an additional polarization emerges as given in Eq. (2), written here as a sum of linear and second-order (in strain) terms: $\boldsymbol{P}^{\mathrm{pz}} = \boldsymbol{P}_1^{\mathrm{pz}} + \boldsymbol{P}_2^{\mathrm{pz}}$. Following Eq. (23) this piezoelectric polarization is defined theoretically as the response function under vanishing macroscopic field $\boldsymbol{E} = 0$, and this is the way it is calculated within DFT. This is a rather theoretical concept since in a crystal an electric field will emerge from the polarization charges. This field would have to be explicitly short-circuited, to fulfill the $\boldsymbol{E} = 0$ condition, which is probably difficult to realize. A discussion on this point can be found, for example, in Ref. 57.

The displacement fields, polarization, and electric fields are related in first order of strain and field via

$$\begin{aligned}
&\boldsymbol{D} = \varepsilon_0 \boldsymbol{E} + \boldsymbol{P},\\
&\boldsymbol{P} = \varepsilon_0 \boldsymbol{\chi}_e \boldsymbol{E} + \boldsymbol{P}_1^{\mathrm{pz}},\\
&\boldsymbol{D} = \varepsilon_0 \boldsymbol{E} + \varepsilon_0 \boldsymbol{\chi}_e \boldsymbol{E} + \boldsymbol{P}_1^{\mathrm{pz}} = \varepsilon_0 \boldsymbol{\varepsilon} \boldsymbol{E} + \boldsymbol{P}_1^{\mathrm{pz}},
\end{aligned}$$

and up to second order in both strain and field via

$$\begin{aligned}
&\boldsymbol{D} = \varepsilon_0 \boldsymbol{E} + \boldsymbol{P},\\
&\boldsymbol{P} = \varepsilon_0 \boldsymbol{\chi}_e \boldsymbol{E} + \varepsilon_0 \boldsymbol{\chi}_e' \boldsymbol{E}^2 + \boldsymbol{P}_1^{\mathrm{pz}} + \boldsymbol{P}_2^{\mathrm{pz}},\\
&\boldsymbol{D} = \varepsilon_0 \boldsymbol{E} + \varepsilon_0 \boldsymbol{\chi}_e \boldsymbol{E} + \varepsilon_0 \boldsymbol{\chi}_e' \boldsymbol{E}^2 + \boldsymbol{P}_1^{\mathrm{pz}} + \boldsymbol{P}_2^{\mathrm{pz}},\\
&\boldsymbol{D} = \varepsilon_0 \boldsymbol{\varepsilon} \boldsymbol{E} + \varepsilon_0 \boldsymbol{\chi}_e' \boldsymbol{E}^2 + \boldsymbol{P}_1^{\mathrm{pz}} + \boldsymbol{P}_2^{\mathrm{pz}}.
\end{aligned}$$

Now two possible experimental situations can occur. If the sample is short circuited $\boldsymbol{E} = 0$ and if it is electrically isolated $\boldsymbol{D} = 0$. For the latter case we obtain in first order

$$\varepsilon_0 \boldsymbol{\varepsilon} \boldsymbol{E} = -\boldsymbol{P}_1^{\mathrm{pz}}, \tag{24}$$

and in second order we obtain

$$\boldsymbol{0} = \varepsilon_0 \boldsymbol{\varepsilon} \boldsymbol{E} + \varepsilon_0 \boldsymbol{\chi}_e' \boldsymbol{E}^2 + \boldsymbol{P}_1^{\mathrm{pz}} + \boldsymbol{P}_2^{\mathrm{pz}}, \tag{25}$$

which would require the calculation of the second-order electric susceptibility tensor:

$$\boldsymbol{\chi}_e' \equiv \chi'_{\alpha\beta\gamma} = \frac{1}{\varepsilon_0}\frac{\partial P_\alpha}{\partial E_\beta \partial E_\gamma}. \tag{26}$$

We neglect the term of second order in the field and write $\varepsilon_0 \boldsymbol{\varepsilon} \boldsymbol{E} = -\boldsymbol{P}_1^{\mathrm{pz}} - \boldsymbol{P}_2^{\mathrm{pz}}$.

Note that the stress and the electric field are coupled via the Navier equation:

$$\boldsymbol{T} = c\boldsymbol{S} - \tilde{e}\boldsymbol{E}, \tag{27}$$

where $\boldsymbol{T}$ is the stress tensor, c the stiffness tensor, $\tilde{e}$ the piezoelectric tensor, and $\boldsymbol{E}$ the electric field.[33] We neglect this coupling, which has been shown to be small.[33]

We apply this formalism to the case of superlattices or QWs, which are structures with periodicity in the growth plane. In this case $\partial/\partial_x = \partial/\partial_y = 0$ (if x, y are in the growth plane) and from Maxwell's equations we obtain for the in-plane electric field, $\boldsymbol{E}_\parallel = 0$. Hence, the electric field is parallel or antiparallel to the growth direction and if the dielectric tensor is diagonal

(as in the zinc blende structure), only the projection of the polarization along the growth axis is relevant.

B. Special case of a [111] quantum well

For zinc-blende III-V semiconductor materials, strain along the [111] axis represents an important case since the polarization $\boldsymbol{P}$ and the piezoelectric field $\boldsymbol{E}$ are directed along the direction of growth (which is not generally the case) and the piezoelectric field is usually the largest (this is only formally true if second-order effects are neglected, but even considering second-order effect it is true in most of the cases). Moreover, the overwhelming majority of previous investigations were performed on structures grown on the (111)-oriented surface. The field and polarization can be reduced to scalar quantities E and P since polarization and electric field are parallel or antiparallel to the growth axis. Using first-order terms in strain for the piezoelectric polarization the piezoelectric field in the well can be calculated from Eq. (4). The strain tensor in this geometry has the following properties: $\eta_4 = \eta_5 = \eta_6$, $\eta_1 = \eta_2 = \eta_3$, and the polarization can be written as

$$P_l^{111} = \sqrt{3} e_{14} \eta_4 = 2\sqrt{3} e_{14} \eta_{xy}. \tag{28}$$

The shear strain can be calculated for pseudomorphic growth from the elastic constants C_{ij}:[58]

$$\eta_{xy} = -\frac{C_{11} + 2C_{12}}{C_{11} + 2C_{12} + 4C_{44}} \varepsilon_{\parallel}, \tag{29}$$

where

$$\varepsilon_{\parallel} = \frac{\delta a}{a} = \frac{a_{\text{sub}} - a_{\text{well}}}{a_{\text{well}}}, \tag{30}$$

where a_{sub} and a_{well} are the lattice constants of the substrate and the well, respectively. Investigating all the material properties entering in Eqs. (28) and (24), we see that the linear regime is appropriate for the dielectric constant[59] given the electric field values involved (hundreds of kV/cm), and the elastic coefficients for strain values up to 2%.[36] The only remaining source of possible nonlinearity is then the piezoelectric constant.

Considering the quadratic dependence of the piezoelectric polarization in strain involves the use of both diagonal and traceless strain components [Eq.(4)]. For [111] growth, the diagonal components can be calculated from the elastic constants as well:

$$\eta_{xx} = \eta_{yy} = \eta_{zz} = \frac{4C_{44}}{C_{11} + 2C_{12} + 4C_{44}} \varepsilon_{\parallel}, \tag{31}$$

and the off-diagonal components are $\eta_{xy} = \eta_{xz} = \eta_{yz}$, as given in Eq. (29).

The polarization from Eq. (2) along the [111] direction becomes

$$P^{111} = \sqrt{3} \left[e_{14} \eta_4 + (B_{114} \eta_1 + 2B_{124} \eta_2) \eta_4 + B_{156} \eta_5 \eta_6 \right], \tag{32}$$

with a linear part given by $P_l^{111} = \sqrt{3} e_{14} \eta_4$ and a nonlinear term: $P_{nl}^{111} = \sqrt{3}(B_{114}\eta_1 + 2B_{124}\eta_2)\eta_4 + B_{156}\eta_5\eta_6$. Note that the polarization P^{111} can be positive or negative if it is parallel or antiparallel to the [111] crystallographic direction.

For ternary compounds we use Vegard's law for the lattice parameters. For the elastic constants, deformation potentials and piezoelectric constants we interpolated between bulk values.

C. General case of a quantum well grown along an arbitrary direction

We describe how to obtain the strain tensor in Cartesian coordinates for a layered zinc-blende structure pseudomorphically gown on a substrate for arbitrary crystallographic growth directions. Pseudomorphic growth means that a semiconductor of lattice constant a_{well} is grown on a substrate of lattice constant a_{sub}. The atomic layers of lattice constant a_{well} on the substrate are facing compressive or tensile strain [depending on the sign of $(a_{\text{sub}} - a_{\text{well}})$] in the growth plane. In the growth direction, the layered zinc-blende structure (the well) is allowed to relax and will do so, according to the elastic properties of the material, fully described by the the fourth-rank elastic tensor $C_{\alpha\beta\gamma\delta}$. To calculate the strain tensor for arbitrary growth direction (hkl), where h,k,l are the Miller indices, we proceed as follows.

(1) We define a rotation matrix $R_{\alpha\beta}$ that transforms the Cartesian coordinate system to a coordinate system where the (hkl) direction represents the z' direction, with x' and y' orthogonal to it and to each other.

(2) In this primed coordinate system, five of the six independent strain tensor elements can be simply derived by symmetry arguments: $\eta'_{xx} = \eta'_{yy} = \delta a/a$, $\eta'_{xy} = 0$, and $\eta'_{xz} \neq \eta'_{yz} \neq 0$. The analytic expressions for η'_{xz} and η'_{yz} can be found in Refs. 60–62 and are not reproduced here. The last element, η'_{zz}, can be obtained by imposing a vanishing stress along the growth direction. The stress and the strain tensors are connected via $\sigma'_{\alpha\beta} = C'_{\alpha\beta\gamma\delta}\eta'_{\gamma\delta}$, which leads to the expression

$$\eta'_{zz} = -\frac{C'_{3311} + C'_{3322}}{C'_{3333}} \frac{\delta a}{a}. \tag{33}$$

(3) The rotated elastic constants needed in Eq. (33) are obtained via the Von Neumann relation of the tensor rotation,

$$C'_{\alpha\beta\gamma\delta} = R_{\alpha\lambda} R_{\beta\mu} R_{\gamma\nu} R_{\delta\xi} C_{\lambda\mu\nu\xi}.$$

(4) Now that the strain tensor in the primed coordinate system is fully defined, we obtain it in the unrotated Cartesian coordinates via $\eta_{\alpha\beta} = R^{-1}_{\alpha\lambda} R^{-1}_{\beta\mu} \eta'_{\lambda\mu}$, where the inverse of a rotation matrix is simply its transpose. Unfortunately, very lengthy expressions are obtained following this procedure. In the Appendix, we give the general analytic expression for the strain tensor we obtain assuming $\eta'_{xz} = \eta'_{yz} = 0$, and discuss how severe this approximation is. The strain tensors for specific common orientations have a rather simple form given as [111] QW $\theta = \tan^{-1}[\sqrt{2}]$, $\phi = \pi/4$,

$$\eta_{xx} = \eta_{yy} = \eta_{zz} = \frac{4C_{44}}{C_{11} + 2C_{12} + 4C_{44}} \frac{\delta a}{a}, \tag{34}$$

$$\eta_{xy} = \eta_{xz} = \eta_{yz} = -\frac{(C_{11} + 2C_{12})}{C_{11} + 2C_{12} + 4C_{44}} \frac{\delta a}{a}; \tag{35}$$

[100] QW $\theta = \pi/2$, $\phi = 0$,

$$\eta_{xx} = -\frac{2C_{12}}{C_{11}} \frac{\delta a}{a}, \tag{36}$$

$$\eta_{yy} = \eta_{zz} = \frac{\delta a}{a}, \tag{37}$$

$$\eta_{xy} = \eta_{xz} = \eta_{yz} = 0; \tag{38}$$

[110] QW $\theta = \pi/2, \phi = \pi/4$,

$$\eta_{xx} = \eta_{yy} = -\frac{(C_{12} - 2C_{44})}{C_{11} + C_{12} + 2C_{44}} \frac{\delta a}{a}, \tag{39}$$

$$\eta_{zz} = \frac{\delta a}{a}, \tag{40}$$

$$\eta_{xy} = -\frac{(C_{11} + 2C_{12})}{C_{11} + C_{12} + 2C_{44}} \frac{\delta a}{a}, \tag{41}$$

$$\eta_{xz} = \eta_{yz} = 0. \tag{42}$$

D. Electrostatic boundary conditions and quantum well superlattices

In [111]-oriented QW superlattices the polarization along the growth direction is piecewise constant in the barrier and in the well. This is equivalent to a distribution of piezoelectric bound charges confined to sheets of charges with uniform density $-P$ on one type of interface and $+P$ on the other. The system thus behaves as an array of parallel capacitors. Using the integral version of Maxwell's equation and applying periodic boundary conditions, which means the superlattice is short circuited in the growth direction, the induced piezoelectric field in the wells reads

$$E = -\frac{P}{\varepsilon_0} \frac{L - t}{t\varepsilon_b + (L - t)\varepsilon_w}, \tag{43}$$

where t is the thickness of the well, L the period of the superlattice, and ε_b and ε_w the static dielectric constants of the barrier and the well materials, respectively. Assuming $\boldsymbol{D} = 0$, which is valid for an isolated sample with no free charges, we obtain

$$E = -\frac{P}{\varepsilon_w \varepsilon_0}, \tag{44}$$

which also represents the limiting case of Eq. (43) for an infinite barrier.

IV. RESULTS FOR PIEZOELECTRIC FIELDS IN [111] QUANTUM WELLS

Using the piezoelectric coefficients and the elastic constants given in Table III we can calculate the piezoelectric fields for different material combinations. From all the possible 72 combinations between the nine III-Vs semiconductors we have chosen 14 based on the requirement of lattice mismatch and the popularity of the material system. The barrier is taken as infinitely thick, following Eq. (44). We show the results in Fig. 3 in the form of bar charts, where we use the notation A/B to describe material A lattice matched to material B. We used pure materials, although some combinations are impossible to grow due to the large lattice mismatch. This figure is clearly an illustration of the effect. The field for a specific QW composition and geometry can be easily calculated from the coefficients. The field using linear coefficients only is given for each QW by the left bar and the field including linear and quadratic terms by the right bar. The effects of the quadratic terms is very large for all the structures, sometimes reversing the sign of the field (InAs/GaAs, InSb/GaSb, InP/InAs, InAs/InP, InSb/InAs). Some structures have very small fields if only the linear terms are accounted for (InP/GaP, InP/InAs) but have significant fields taking second-order coefficients into account. Some QWs exhibit very large fields up to few MV/cm, such as GaP/InP or GaAs/InAs.

TABLE III. Elastic constants in units of 10^{11} dyne cm^{-2} calculated via DFT and used in the calculation of the piezoelectric fields in QWs.

	AlP	AlAs	AlSb	GaP	GaAs	GaSb	InP	InAs	InSb
C_{11}	13.29	11.22	8.56	14.06	11.33	8.92	9.89	8.28	6.70
C_{12}	6.75	5.53	4.25	6.18	5.08	3.97	5.56	4.66	3.63
C_{44}	6.29	5.43	3.96	6.90	5.68	4.43	4.47	3.74	3.05

V. RESULTS FOR PIEZOELECTRIC FIELDS IN $IN_xGA_{1-x}AS/GAAS$ QUANTUM WELLS FOR ARBITRARY GROWTH DIRECTION

We have expressed the polarization from Eq. (2) in spherical coordinates using the general form of the strain tensor for pseudomorphic growth, as described in Sec. III C. This allows us to calculate the polarization for any growth direction (hkl). From the polarization we obtain the piezoelectric field using Eq. (43), where the scalar P is the projection of the polarization on the vector $\boldsymbol{r}$,

$$P = \boldsymbol{P} \cdot \hat{\boldsymbol{r}},$$

where $\hat{\boldsymbol{r}}$ is along the growth direction and is given as a function of Euler angles as $(\sin\theta\cos\phi,\ \sin\theta\sin\phi,\ \cos\theta)$. In this section, we show results for an $In_xGa_{1-x}As$ QW with a thickness of 10 nm, pseudomorphically grown on GaAs. For the dielectric constants we used $\varepsilon_{InAs} = 15.15$ and $\varepsilon_{GaAs} = 12.90$. The elastic, lattice, and dielectric constants are

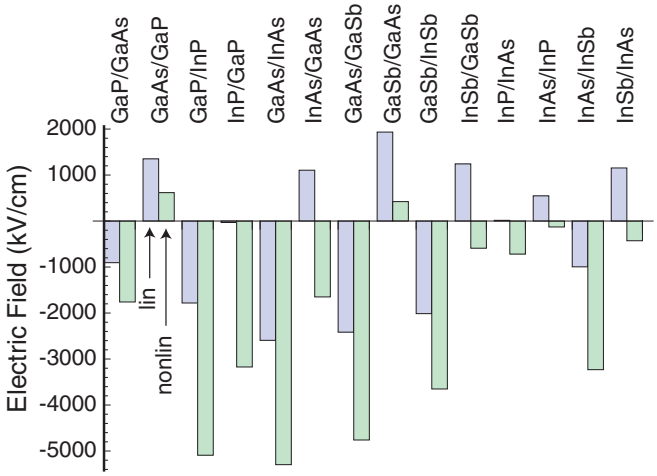

FIG. 3. (Color online) Bar charts of the piezoelectric fields for 14 different QWs A/B, where the material A is strained to the lattice constant of material B. The barrier is taken as infinitely thick [Eq. (44)]. The left (right) bar for each QW represents the result taking only the linear (both the linear and quadratic) term(s) into account.

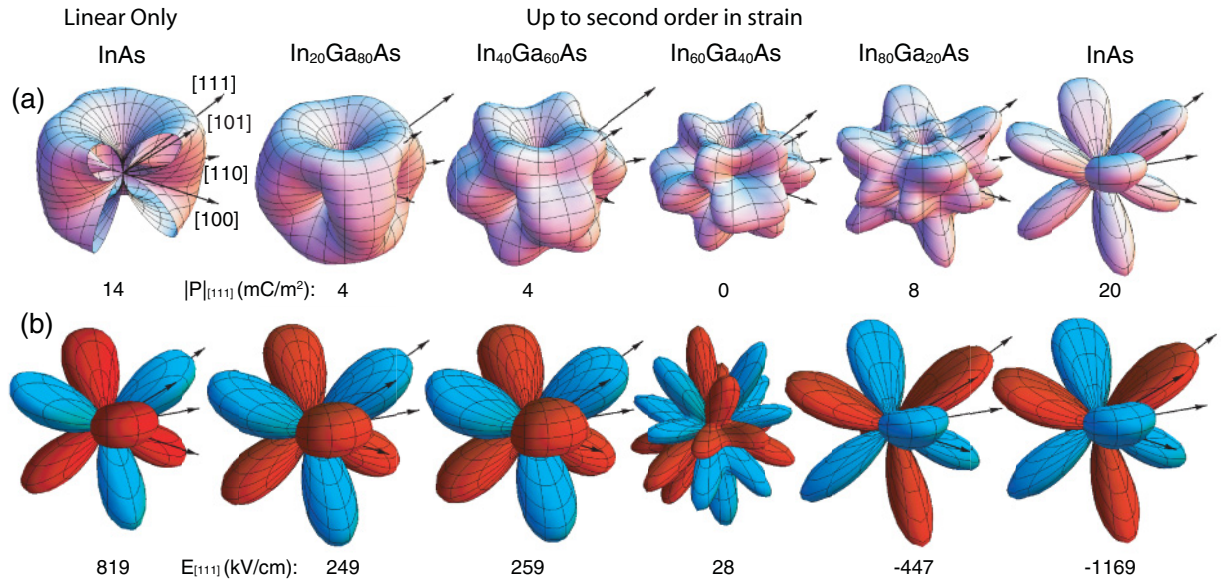

FIG. 4. (Color online) Spherical polar plots of the magnitude of the polarization (a) and of the piezoelectric field (b) in pseudomorphic $In_xGa_{1-x}As/GaAs$ QWs of arbitrary crystallographic orientation. The wells are 10 nm wide and surrounded by 30-nm GaAs barriers. The Euler angles θ and ϕ give the direction of the growth axis according to Eqs. (A1), and at the same time the orientation of the piezoelectric field. The radial dimension of the spherical polar plot gives the absolute value of the length of the polarization vector (a) and the piezoelectric field along the growth direction (b). The blue and red colors in (b) indicate if the field is oriented parallel or antiparallel to the growth direction, respectively. The numerical values of the magnitude of the polarization and of the piezoelectric fields along the [111] direction are given at the bottom of each plot. Note that the field $E_{[111]}$ (for [111] growth) is oriented along the growth direction for In concentrations up to 60% but is reversed for 80% and 100% In concentrations. The spherical polar plots considering only the linear term are qualitatively the same for all concentrations and only the pure InAs case is shown on the left. With linear term only for the concentrations 20%, 40%, 60%, 80%, 100% the values of the field are 324, 561, 720, 804, 819 kV/cm, respectively, and for the magnitudes of the polarizations we obtain 5, 9, 12, 13, 14 mC/cm^2.

averaged between bulk values when we calculate the random alloys. In Fig. 4(a) we have plotted the magnitude of the polarization in a spherical polar plot where the Euler angles θ and ϕ give the direction of the growth axis according to Eqs. (A1). In a similar fashion we have plotted in Fig. 4(b) the piezoelectric field including only the linear term [leftmost plot in Fig. 4(b)] and also including the linear and nonlinear terms for various In concentrations. On the grounds of symmetry, the polarization vanishes for the {100} directions. If only the linear terms are included, the magnitude of the polarization shows sharp dips around the {100} directions but, aside from these steep depressions, is rather homogeneous. For instance, the difference between the magnitude of the polarization along the [111] and [110] directions is only 8%. The piezoelectric field in Fig. 4(b) is qualitatively different as it vanishes also along the {110} directions. In this case the polarization is perpendicular to the growth direction and does not allow for the field to develop. So the {100} directions are nonpiezoelectric because of the symmetry of the strain tensor (no shear strain components), while the {110} directions are nonpiezoelectric because the polarization is orthogonal to the growth direction. If only the linear terms are considered, the shape of the polar plots of the polarization and field do not change qualitatively, when changing the concentration, and we therefore show only one image for the pure InAs case. The magnitude of the polarization and field, however, does increases as the strain becomes larger, moving to higher In concentrations. We obtain for the concentrations $x = 0.2, 0.4, 0.6, 0.8, 1.0$ the fields 324, 561, 720, 804, 820 in kV/cm and the polarizations 5, 9, 12, 13, 14 mC/m^2 along the [111] direction, respectively.

Including the second-order terms (six images on the right of Fig. 4) changes the images qualitatively. At 20% In concentration, the shape is still similar to the shape obtained with linear coefficients only, although the field has shrunk by 23% (from 324 to 250 kV/cm). Further increase in concentration changes the morphology of the surface plot and its magnitude. At around 60% the sign of the field for [111]-growth changes, so that the field is now oriented toward the $[\bar{1}\bar{1}\bar{1}]$ direction. The second-order terms make the surface extremely anisotropic. The field along the {111} directions reaches the MV/cm. This represents, however, the extreme case of a pure InAs QW, which cannot be grown pseudomorphically on GaAs. Such values of strain can only be obtained in quantum dot structures,[38] but also there the structures are usually alloyed with overall concentrations around 60%. At this concentration the expected field is very small (36 kV/cm, much smaller than if only the linear terms were considered: 720 kV/cm), but it becomes clear that small deviations from a nominal composition of 60% will boost up the piezoelectric field significantly.

VI. EXPERIMENTAL DETERMINATION OF PIEZOELECTRIC FIELDS

The experimental determination of the piezoelectric field is an intricate and indirect process. The simple measurement

of the deformation of the crystal under applied voltage via interferometric techniques is possible, but the results depend heavily on the sample morphology and used apparatus (see, e.g., Ref. 63). Other methods are indirect and based on approximations sometimes difficult to gauge. We critically present the most common techniques and related issues.

A. Determination from optical spectra

Photoluminescence (PL) has been used extensively to characterize heterostructures and piezoelectric field effects.[64–69] In fact, PL and absorption spectra give indications about the spatial separation of electrons and holes in the presence of strain-induced electric field: The transition probability between electron and hole states in a QW is reduced and its transition energy is also lowered due to the separation of electrons and holes and the quantum-confined Stark effect. The measurement of both effects makes it possible, in principle, to determine the built-in field. Since the composition of the QW generally fluctuates, the calculation of one transition energy cannot be directly compared with the measurements. The transition energy is therefore measured as a function of a parameter. Four main possibilities have been explored: (1) varying the well width, (2) varying the QW composition, (3) varying the optical excitation power and hence the density of screening charges,[70–74] or (4) applying an external voltage and looking for the flat-band condition, when the PL intensity and transition energy are maximum.[63,75–77]

B. Local minima lead to interface charges

In multiquantum well (MQW) structures, the observed blueshifts were attributed to another mechanism.[78] Depending on the geometry of the structure, an internal field can sometimes be created across the MQW, giving rise to local minima in the potential at either end of the MQW and trapping photogenerated carriers that have escaped from the QWs and have drifted to the edges of the MQW region. Many PL and time-resolved absorption measurements are consistent with this model,[78–84] but they do not provide quantitative information about the internal position of the screening charges. Generally both in-well and out-of-well screening can occur in such structures and, the estimate of piezoelectric field strength from the variation in transition energy only cannot yield reliable results.

C. The calculation of transition energies depends on several nontrivial aspects

Several processes responsible for both the redshifts and the blueshifts can occur simultaneously making interpretation of the PL complicated. The redshifts seen at low excitation power are attributed to the photovoltaic effect in piezoelectric strained InGaAs-GaAs MQW p-i-n structures,[85] while the blueshifts are attributed to competing effects of band-gap renormalization (quantum confinement), band-state filling and partial carrier screening of the piezoelectric field in InGaAs QWs grown on (111)*B* (Refs. 28,86, and 87) and (111)*A* (Refs. 88 and 89) GaAs substrates. However, even at low optical power, that is, at negligible carrier densities, big differences still appear and are thought to be due to strain relaxation, charge trapping, and defects at the interfaces.[88,89] For doped samples, the possibility that the piezoelectric field is screened by free charges supplied from the substrate (for example, $n+$ GaAs substrate in Ref. 90) cannot be completely ruled out. These uncertainties are probably in the same order of magnitude as the theoretical uncertainties for materials with a vanishing gap in the LDA or GGA approximations (InAs, GaSb, InSb), as mentioned in Sec. II E.

D. Dielectric models are often not appropriate

As described, most of the measurements determine the internal field. To extract the piezoelectric constant from the measured value of the field, Eqs. (28) and (44) are most often used. According to that equation, the piezoelectric field does neither depend on the layer thickness nor on the barrier width, which is true only for infinitely large barriers, or for electrically isolated wells. This equation is, however, often used for MQW structures, which is obviously inappropriate. From Eq. (43) it is clear that well and barrier thicknesses are very much relevant in these cases. One must also realize that Eq. (43) represents in most cases an approximation as well. The determination of the electric field in the well requires the solution of the electrostatic problem with the appropriate boundary conditions and taking doping layers into account. These ideas have been considered in the case of a multiple quantum well in p-i-n structures in which the in-well field in the active region is calculated as a combined result of the built-in voltage, due to the different doping levels of the p and n regions.[84,85] However, these models have been used in only few cases and it is often not clear what electrostatic model was used to derive the field.

E. Accuracy of the bulk values e_{14}^{exp}

The discrepancy between the value of the piezoelectric constant deduced from $In_xGa_{1-x}As/GaAs$ QW measurements and the value deduced from the linear interpolation between the bulk values e_{14}^{exp} has been constantly reported in the literature. In addition to the reasons already mentioned above, such a disagreement could be due to an approximate knowledge of the piezoelectric constants of the binary constituents. All the piezoelectric constants determined from bulk materials (reported in Table I as e_{14}^{exp}) originate from one paper by Arlt and Quadflieg[91] with subsequent papers attempting to model their data (e.g., Ref. 92). It seems reasonable, and has already been suggested by Tober and Bahder,[93,94] to question the accuracy of the determined piezoelectric constants. Possible errors due to charge accumulations at the interfaces screening the electric field cannot be ruled out.

VII. COMPARISON WITH EXPERIMENT

In Table IV we have summarize the results we found in the literature along with the theoretical results. The overwhelming majority of reports for III-V materials are for $In_xGa_{1-x}As$ wells, epitaxially grown on GaAs. The combination InAs/GaAs offers a rather large lattice mismatch of 7% and cannot be grown as pure materials. The achievable limit for the In concentration is around $x \simeq 0.2$ for defect-free growth. This brings down the lattice mismatch below 2%, still enough to develop rather large piezoelectric fields. In Table IV we

TABLE IV. Experimental results collected in the literature and theoretical results using the piezoelectric bulk coefficients[107] (e_{14}^{exp}), our linear coefficients only (lin), and the linear plus quadratic coefficients (nonlin).

			Piezoelectric field (kV/cm)				
				Theory			
Sample	Well	Barrier	Experiment	$e_{14}^{\mathrm{exp.}}$	lin	nonlin	References
S1	$In_{0.20}Ga_{0.80}As$ (10 nm)	$Al_{0.35}Ga_{0.65}As$ (50 nm)	154	257	404	**301**	88
S2	$In_{0.23}Ga_{0.77}As$ (10 nm)	GaAs (100 nm)	240	342	462	**331**	87
S3	$In_{0.15}Ga_{0.85}As$	GaAs	220 ± 50	210	350	**289**	96
S4	$In_{0.15}Ga_{0.85}As$ (7 nm)	GaAs (14 nm)	200	178	235	**194**	78
S5	$In_{0.15}Ga_{0.85}As$	GaAs	$\sim$200	220	242	**200**	97
S6	$In_{0.15}Ga_{0.85}As$ (10 nm)	GaAs (15 nm)	166	237	212	**175**	85
S7	$In_{0.17}Ga_{0.83}As$ (9.5 nm)	GaAs (14.5 nm)	135	192	239	**191**	84
S8	$In_{0.15}Ga_{0.85}As$ (10 nm)	GaAs (15 nm)	155	227	212	**175**	98
S9	$In_{0.13}Ga_{0.87}As$ (4.1 nm)	GaAs	131	196	307	**262**	99
S10	$In_{0.17}Ga_{0.83}As$ (8.7 nm)	GaAs	170	246	391	**313**	100
S11	$In_{0.17}Ga_{0.83}As$ (10 nm)	GaAs	160	246	391	**313**	101
S12	$In_{0.21}Ga_{0.79}As$ (10 nm)	GaAs	166	292	469	**349**	102
S13	$In_{0.21}Ga_{0.79}As$ (2–16 nm)	GaAs (50 nm)	145	254–287	358–452	**267–337**	10
S14	$In_{0.10}Ga_{0.90}As$ (10 nm)	GaAs	170	155	242	**215**	103
S15	$In_{0.055}Ga_{0.945}As$ (25 nm)	GaAs (50 nm)	90	89	101	**94**	104
S16	$In_{0.15}Ga_{0.85}As$ (10 nm)	GaAs (15 nm)	165	167	212	**175**	105
S17	GaAs (13.1 nm)	$GaAs_{0.87}P_{0.13}$ (58.6 nm)	220	88	136	**146**	32
S18	$In_{0.53}Ga_{0.47}As$ (17.5 nm)	$Al_{0.70}In_{0.30}As$ (35 nm)	141	192	312	**188**	106
S19	$In_{0.53}Ga_{0.47}As$ (17.5 nm)	$Al_{0.26}In_{0.74}As$ (35 nm)	137	−123	−234	**−308**	106
S20	$In_{0.24}Ga_{0.76}As$ (10 nm)	GaAs (100 nm)	149	320	464	**330**	28
S21	$In_{0.28}Ga_{0.72}As$ (10 nm)	GaAs (100 nm)	146	360	527	**343**	28
S22	$In_{0.33}Ga_{0.67}As$ (10 nm)	GaAs (100 nm)	131	404	598	**343**	28

indicate the barrier and well width, in case it was reported, and calculate the piezoelectric fields according to Eq. (43). In case no such width is reported we assumed infinite wells and used Eq. (44), with the exception of S5 that refers to an experiment performed on a MQW structure and assuming Eq. (28) would be unreasonable. For this structure we chose 10 nm for the well width and 22 nm for the barrier thickness. We are comparing, whenever possible, the measured field rather than the piezoelectric coefficients, as the latter are extracted from the field using some models and are indirect. We report three different values of theory: one ($e_{14}^{\mathrm{exp.}}$ column) where we report the value provided in the corresponding paper or, in case this value was not reported, the value we calculate using only the linear coefficients of Arlt and Quadflieg,[91] the other using our linear coefficients only (lin) and finally using our linear and quadratic coefficients (nonlin).

The general trend discussed in the literature, that the measured fields are lower than the ones calculated based on the coefficients, is confirmed in general. However, from the 22 measurements reported, 7 show rather good agreement between theory and experiment. Others show a measured field up to a factor of two smaller than the calculated values (S1, S13, S19, S20, S21, S22). A quantitative comparison among experimental results is difficult because of the disparity in the structures studied. However, we can directly compare S6, S8, and S16 and find a rather modest discrepancy of 11 kV/cm. A similar discrepancy is found in the case of S10 and S11, with a deviation of 10 kV/cm. It seems that experiments performed on less strained samples agree better with the theory. For instance, S15 agrees well with the theory. The samples S20, S21, S22 show strong disagreement with the theory, but the trend to have at these high In compositions a composition-independent field is reproduced by our results, although the numerical values are higher. This behavior is due to the nonlinear term, as is illustrated in Sec. VIII.

VIII. DEPENDENCE ON THE In CONCENTRATION AND THE WELL GEOMETRY

Although it is clear from Eq. (43) that the well and barrier thicknesses enter the equation for the electric field, it is sometimes omitted. In Ref. 95, for instance, theoretical and experimental piezoelectric effects were reported and, for a multiple quantum well structure consisting of 8-nm $In_{0.2}Ga_{0.8}As$ wells and 10-nm of GaAs barriers, the piezoelectric field (higher than 300 kV/cm) was found from Eq. (28) as a function of the indium concentration x. Though the barrier and well thicknesses were comparable, that work did not take it into account. As expected from Eq. (43) and shown in Fig. 5, the field strength is also an outcome of the layer thicknesses ratio for periodic structures. Thus, uncertainty on the layer thickness or analysis carried out without regard to the thickness may also influence the experimental results reported.

We show in Fig. 6 for an InAs/GaAs QW that the second-order contribution induces a sign change in the field. Retaining only the linear contribution from Table I leads to a monotonously increasing field with increasing In content, until a maximum value E_{max} is reached around $x = 1$. In

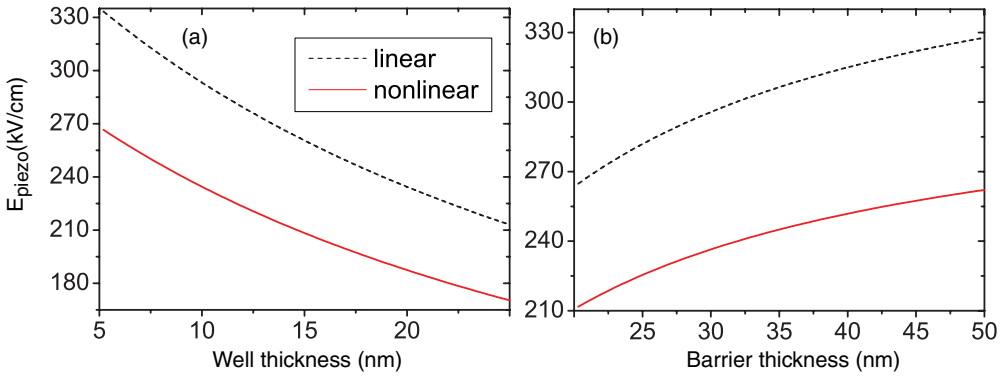

FIG. 5. (Color online) (Left) $In_{0.17}Ga_{0.83}As/GaAs$. Strain-induced field (kV/cm) in the QW as a function of the well width, calculated with linear (dashed line) and nonlinear (solid line) piezoelectric constants. The barrier width is fixed at 29 nm. (Right) Piezoelectric field as a function of the barrier width for a well thickness fixed at 10 nm.

fact, this behavior is closely linked to the configuration chosen. The general trend is a decrease of the field after the maximum has been attained. Increasing x beyond the value corresponding to E_{max} does not result in higher fields. When the second-order terms are taken into account, the maximum field value is attained at much lower In fraction. This behavior is in qualitative agreement (although our fields are quantitatively higher) with the series S20, S21, S22 in Table IV. The In concentration was varied in the range of 24% to 33% with no significant change in the piezoelectric field.

IX. DISCUSSION

Before we conclude we address some possible issues and open questions. From the sections devoted to the description of experimental procedures and to the comparison with experiment it seems reasonable to assume that the measured fields are, to some extent, screened. This is based on the fact that some experiments agree very well with the theory, suggesting that high fields *can* be produced. The complementary argument is heuristic and based on the assumption that any imperfections would lower the field, rather than increase it. While this seems a reasonable conclusion, possible errors in the calculation should be pointed out. (1) The basis of density functional theory, as we have used it, is the local approximation to the exchange correlation (LDA). Severe deficiencies are known to ensue from this approximation, such as wrong band gaps, effective masses, and Dresselhaus spin splittings along with a wrong energetic position of d states, all of these being interrelated. As previously discussed (Sec. II E), the results for the linear coefficients for materials with vanishing band gap in the LDA/GGA approximations (InAs, GaSb, InSb) are shadowed by uncertainties. Especially, we cannot exclude at the moment that the e_{14} coefficient for InAs may be close to the experimental value of Arlt and Quadflieg.[91] We notice that assuming the experimental value for the linear term would bring the piezoelectric fields for QWs in excellent agreement with most experiments. On the other hand, elastic properties are quite well behaved and have led to impressive predictions, especially for phonons. Phonons are, much like the piezoelectric effect, driven by the electronic response to a mechanical deformation. So we have no *a priori* reason to doubt the applicability of LDA or GGA. (2) Another issue is the assumption in the calculation of piezoelectric fields for QWs of a linear interpolation between bulk values for alloyed materials. This approach is rather accurate for lattice constants (Vegard's law) but certainly represents an approximation for piezoelectric coefficients, where we expect a certain degree of nonlinearity (bowing). As the comparison with experiment does not yield the necessary accuracy, we would suggest *ab initio* calculations based on special quasirandom structures (SQSs). These structures reproduce some alloy properties while keeping the number of atoms low. Such an approach was recently taken[108] to obtain elastic coefficients of alloys and earlier for the linear piezoelectric coefficients of nitrides.[109] (3) One last comment is related to details of the structure. Some interdiffusion at the interface between the materials was suggested by Ballet *et al.*[110] and cannot be ruled out. This uncertainty is to be added to the uncertainty given in the nominal width of barriers and wells.

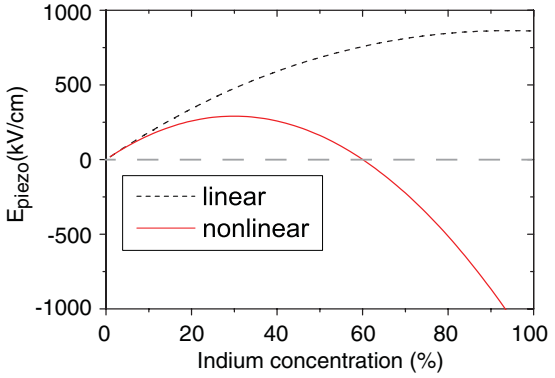

FIG. 6. (Color online) Piezoelectric field (kV/cm) in $In_xGa_{1-x}As/GaAs$ QW as a function of the indium concentration x. Dashed line, only the linear constants from Table I; solid line, the nonlinear constants are included. Well width = 10 nm and barriers width = 30 nm.

X. SUMMARY

We have calculated the first- and second-order (in strain) piezoelectric coefficients for nine binary III-V semiconductors based on *ab initio* DFPT. We derive the relation between the proper and the improper second-order coefficients and outline

a simple calculational procedure. We have tested the reliability of the results by using different types of pseudopotentials and exchange correlation functionals. We assess the parameters to be reliable with some remaining uncertainties on the the linear terms for the materials with vanishing gap at the LDA/GGA level (InAs, GaSb, InSb). We confirm previous *ab initio* results[37,38] that the piezoelectric effect of second order in strain is an important component of the piezoelectric field and cannot be omitted. We show that this is valid for all the calculated materials: GaAs, GaP, GaSb, InAs, InP, InSb, AlAs, AlP, and AlSb. We calculate the strain tensor for pseudomorphic growth along arbitrary crystal directions. This allows us to study the anisotropy of the piezoelectric field with respect to growth directions. We find a significant increase in anisotropy when the second order is included. A careful survey of the experimental literature shows that the measured fields are in most experiments lower than our theoretical predictions, although some measurements are in very good agreement. Possible reasons for this have been discussed, mostly pointing to the possibility of the existence of screening charges and the use of inappropriate electrostatic models, along with the questionable assumption of negligible bowing in the piezoelectric coefficients.

ACKNOWLEDGMENTS

A.B.W. acknowledges support from the Alexander von Humboldt Foundation for a travel grant. G.B. acknowledges fruitful discussions with Yann-Michel Niquet and Peter Vogl. We thank Laurent Pedesseau for giving us his unpublished data on the B_{156} coefficient for InAs.

APPENDIX

We give the expressions for the strain tensor for an arbitrary growth direction (hkl), assuming vanishing shear strain components in the rotated frame: $\eta'_{xz} = \eta'_{yz} = 0$. This represents an approximation in the case of low-symmetry directions that leads to errors in the polarization along these directions. In Fig. 7 we show the difference between the approximate result using $\eta'_{xz} = \eta'_{yz} = 0$ (dashed line) and the accurate result taking the full dependence of η'_{xz} and η'_{yz} into account[60–62] (solid line). Related approaches to this problem with more details can be found in Refs. 60–62 and 111. As shown in Fig. 7 the qualitative behavior of the magnitude of the polarization is similar for the approximate and the exact results, and, indeed, the spherical plots from Fig. 4 appear qualitatively very similar (and quantitatively identical for the high-symmetry growth directions) using either of the approaches (not shown). However, quantitative differences in the magnitude of the polarization can be quite significant for specific directions. For instance, in the [113] growth direction (De Caro and Tapfer[62] highlighted that for this direction the shear strain component η'_{xz} is largest), the polarization is significantly modified by the neglect of shear strain.

The connections between the Miller indices (hkl) and the angles θ,ϕ is given by

$$\theta = \tan^{-1}\left[\frac{\sqrt{h^2+k^2}}{l}\right], \quad \phi = \tan^{-1}[k/h], \qquad \text{(A1)}$$

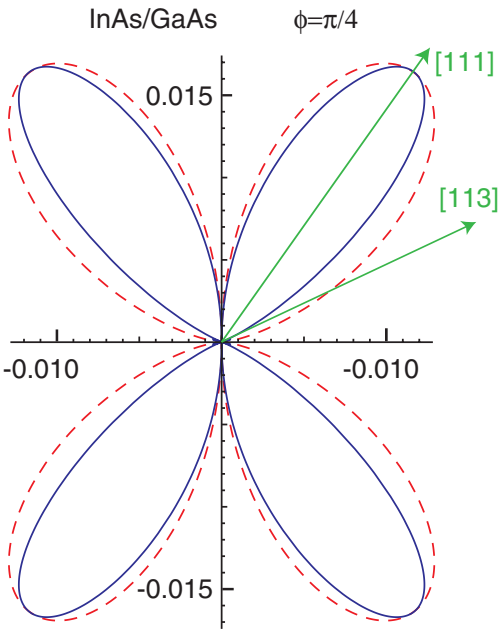

FIG. 7. (Color online) Polar plots of the magnitude of the polarization (in C/m^2) for an InAs QW pseudomorphically grown on GaAs with $\phi = \pi/4$ and varying angle θ (measured from the apex). The dashed line is the result assuming $\eta'_{xz} = \eta'_{yz} = 0$ and the solid line corresponds to the correct result with $\eta'_{xz} \neq \eta'_{yz} \neq 0$.

and we give the results as a function of these Euler angles:

$$\eta_{xx} = \frac{\delta a}{a}\left(\sin^2[\phi] + \frac{\cos^2[\phi]\,(A + B\cos[2\theta] + C)}{D}\right),$$

$$\eta_{xy} = \frac{\delta a}{a}\left(-\frac{E\sin[2\phi]\sin^2[\theta]}{D}\right),$$

$$\eta_{xz} = \frac{\delta a}{a}\left(-\frac{E\cos[\phi]\sin[2\theta]}{D}\right),$$

$$\eta_{yy} = \frac{\delta a}{a}\left(\cos^2[\phi] + \frac{\sin^2[\phi]\,(A + B\cos[2\theta] + C)}{D}\right),$$

$$\eta_{yz} = \frac{\delta a}{a}\left(-\frac{E\sin[\phi]\sin[2\theta]}{D}\right),$$

$$\eta_{zz} = \frac{\delta a}{a}\left(\frac{A - 4(3C_{11} + 9C_{12} + 2C_{44})\cos[2\theta] + C}{D}\right),$$

$$A = 5C_{11} - 21C_{12} + 22C_{44},$$

$$B = 4(5C_{11} + 7C_{12} - 2C_{44}),$$

$$C = (C_{11} - C_{12} - 2C_{44})(7\cos[4\theta] + 8\cos[4\phi]\sin^4[\theta]),$$

$$D = 21C_{11} + 11(C_{12} + 2C_{44}) + (C_{11} - C_{12} - 2C_{44}) \times (4\cos[2\theta] + 7\cos[4\theta] + 8\cos[4\phi]\sin^4[\theta]),$$

$$E = 16(C_{11} + 2C_{12}). \qquad \text{(A2)}$$

With this general expression (within the approximation $\eta'_{xz} = \eta'_{yz} = 0$), the polarization or the piezoelectric field can be calculated for an arbitrary growth direction using linear and second-order piezoelectric coefficients.

*g.bester@fkf.mpg.de

[1] D. L. Smith, Solid State Commun. **57**, 919 (1986).
[2] D. L. Smith and C. Mailhiot, J. Vac. Sci. Technol. A **5**, 2060 (1987).
[3] D. L. Smith and C. Mailhiot, Phys. Rev. Lett. **58**, 1264 (1987).
[4] C. Mailhiot and D. L. Smith, Phys. Rev. B **35**, 1242 (1987).
[5] C. Mailhiot and D. L. Smith, J. Vac. Sci. Technol. A **7**, 609 (1989).
[6] D. L. Smith and C. Mailhiot, Rev. Mod. Phys. **62**, 173 (1990).
[7] D. L. Smith and C. Mailhiot, J. Appl. Phys. **63**, 2717 (1988).
[8] S. de Gironcoli, S. Baroni, and R. Resta, Phys. Rev. Lett. **62**, 2853 (1989), and references therein.
[9] S. de Gironcoli, S. Baroni, and R. Resta, Ferroelectrics **111**, 19 (1990), and references therein.
[10] X. Chen, C. H. Molloy, D. A. Woolf, C. Cooper, D. J. Somerford, P. Blood, K. A. Shore, and J. Sarma, Appl. Phys. Lett. **67**, 1393 (1995).
[11] Cooper, D. I. Westwood, and P. Blood, Appl. Phys. Lett. **69**, 2415 (1996).
[12] Ishihara and H. Watanabe, Jpn. J. Appl. Phys. **33**, 1361 (1994).
[13] Y. M. Niquet, Nano Lett. **7**, 1105 (2007).
[14] M. Zervos and L.-F. Feiner, J. Appl. Phys. **95**, 281 (2004).
[15] G. Klimeck, S. Ahmed, N. Kharche, M. Korkusinski, M. Usman, and M. Prada, IEEE Trans. Electron Devices **54**, 2009 (2007).
[16] W. Ma, X. Wang, Z. Wang, M. L. Hussein, J. Shultz, M. Xiao, and G. J. Salamo, Phys. Rev. B **67**, 035315 (2003).
[17] G. Bester and A. Zunger, Phys. Rev. B **71**, 045318 (2005).
[18] J. Even, F. Doré, C. Cornet, L. Pedesseau, A. Schliwa, and D. Bimberg, Appl. Phys. Lett. **91**, 122112 (2007).
[19] A. Schliwa, M. Winkelnkemper, A. Lochmann, E. Stock, and D. Bimberg, Phys. Rev. B **80**, 161307 (2009).
[20] J. Andrzejewski, G. Sek, E. O'Reilly, A. Fiore, and J. Misiewicz, J. Appl. Phys. **107**, 073509 (2010).
[21] R. D. Underwood, S. Kozodoy, P. Keler, S. P. DenBaars, and U. K. Mishra, Appl. Phys. Lett. **73**, 405 (1998).
[22] T. D. Wen, L. P. Xu, J. J. Xiong, W. D. Zhang, Mingzhong Wu, and H. D. Hochheimer, J. Appl. Phys. **102**, 113703 (2007).
[23] H. S. Kim, J. Y. Lin, H. X. Jiang, W. W. Chow, A. Botchkarev, and H. Morkoc, Appl. Phys. Lett. **73**, 3426 (1998).
[24] K. Omae, Y. Kawakami, S. Fujita, M. Yamada, Y. Narukawa, and T. Mukai, Phys. Rev. B **65**, 073308 (2002).
[25] D. L. Smith, S. M. Kogan, P. P. Ruden, and C. Mailhiot, Phys. Rev. B **53**, 1421 (1996).
[26] S. Adachi, *Physical Properties of III-V Semiconductor Compounds: InP, InAs, GaAs, InGaAs, and InGaAsP* (Wiley & Sons, New York, 1992).
[27] V. C. Stergiou, N. T. Pelekanos, and Y. S. Raptis, Phys. Rev. B **67**, 165304 (2003).
[28] L. Borruel, J. M. Ulloa, J. J. Sanchez, B. R. Herrero, J. Temmyo, J. M. G. Tijero, J. L. Sanchez-Rojas, and I. Esquivias, in *Physics and Simulation of Optoelectronic Devices IX* edited by Y. Arakawa, and P. Blood, M. Osinski, Proceedings of Spie (SPIE-International Society for Optical Engine, Bellingham, WA, 2001), Vol. 4283, pp. 215–226.
[29] E. A. Khoo, A. S. Pabla, J. Woodhead, J. P. R. David, R. Grey, and G. J. Rees, IEE Proc. Optoelectron **145**, 62 (1999).
[30] E. A. Khoo, J. Woodhead, J. P. R. David, R. Grey, and G. J. Rees, Electron. Lett. **35**, 150 (1999).
[31] V. Ortiz and N. T. Pelekanos, Appl. Phys. Lett. **77**, 788 (2000).
[32] X. Zhang, K. Karaki, H. Yaguchi, K. Onabe, R. Ito, and Y. Shiraki, Appl. Phys. Lett. **64**, 1555 (1994).
[33] L. C. Lew Yan Voon and M. Willatzen, J. Appl. Phys. **109**, 031101 (2011).
[34] J. Cibert, R. André, C. Deshayes, L. S. Dang, H. Okumura, S. Tatarenko, G. Feuillet, P. H. Jouneau, R. Mallard, and K. Saminadayar, J. Cryst. Growth **117**, 424 (1992).
[35] R. André, J. Cibert, Le Si Dang, J. Zeman, and M. Zigone, Phys. Rev. B **53**, 6951 (1996).
[36] A. Dal Corso, R. Resta, and S. Baroni, Phys. Rev. B **47**, 16252 (1993).
[37] G. Bester, X. Wu, D. Vanderbilt, and A. Zunger, Phys. Rev. Lett. **96**, 187602 (2006).
[38] G. Bester, A. Zunger, X. Wu, and D. Vanderbilt, Phys. Rev. B **74**, 081305 (2006).
[39] A. Schliwa, M. Winkelnkemper, and D. Bimberg, Phys. Rev. B **76**, 205324 (2007).
[40] L. Pedesseau, J. Even, F. Doré, and C. Cornet, AIP Conf. Proc. **963**, 1331 (2007).
[41] S. P. Lepkowski, Phys. Rev. B **77**, 155327 (2008).
[42] H. Grimmer, Acta Crystallogr. Sect. A **63**, 441 (2007).
[43] V. A. Koptsik, *Shubnikov Groups* (Izd. MGU, Moscow, 1966) [in Russian].
[44] D. F. Nelson, *Electric, Optic, and Acoustic Interactions in Dielectrics* (Wiley, New York, 1979).
[45] ABINIT is a common project of the Université Catholique de Louvain, Corning Incorporated, and other contributors [http://www.abinit.org]; See X. Gonze *et al.*, Comput. Phys. Commun. **180**, 2582 (2009); Z. Kristallogr. **220**, 558 (2005).
[46] N. Troullier and J. L. Martins, Phys. Rev. B **43**, 1993 (1991).
[47] M. Fuchs and M. Scheffler, Comput. Phys. Commun. **119**, 67 (1999).
[48] C. Hartwigsen, S. Goedecker, and J. Hutter, Phys. Rev. B **58**, 3641 (1998).
[49] X. Wu, D. Vanderbilt, and D. R. Hamann, Phys. Rev. B **72**, 035105 (2005).
[50] D. R. Hamann, X. Wu, K. M. Rabe, and D. Vanderbilt, Phys. Rev. B **71**, 035117 (2005).
[51] D. Vanderbilt, J. Phys. Chem. Solid **61**, 147 (2000)
[52] L. Pedesseau (private communication).
[53] W. A. Harrison, Phys. Rev. B **10**, 767 (1974).
[54] W. A. Harrison, Phys. Rev. B **8**, 4487 (1973).
[55] F. Bernardini, V. Fiorentini, and D. Vanderbilt, Phys. Rev. B **56**, R10024 (1997).
[56] M. A. Migliorato, D. Powell, A. G. Cullis, T. Hammerschmidt, and G. P. Srivastava, Phys. Rev. B **74**, 245332 (2006).
[57] R. Resta, J. Phys. Condens. Matter **22**, 123201 (2010).
[58] J. F. Nye, *Physical Properties of Crystals* (Clarendon, Oxford, 1957).
[59] R. Resta and K. Kunc, Phys. Rev. B **34**, 7146 (1986).
[60] E. Anastassakis, Phys. Rev. B **46**, 4744 (1992).
[61] L. De Caro and L. Tapfer, Phys. Rev. B **48**, 2298 (1993).
[62] L. De Caro and L. Tapfer, Phys. Rev. B **51**, 4374 (1995).
[63] M. Feneberg and K. Thonke, J. Phys. Condens. Matter **19**, 403201 (2007).
[64] B. K. Laurich, K. Elcess, C. G. Fonstad, J. G. Beery, C. Mailhiot, and D. L. Smith, Phys. Rev. Lett. **62**, 649 (1989).
[65] T. S. Moise, L. J. Guido, R. C. Barker, J. O. White, and A. H. Kost, Appl. Phys. Lett. **60**, 2637 (1992)
[66] T. S. Moise, L. J. Guido, and R. C. Barker, Phys. Rev. B **47**, 6758 (1993).

[67]T. G. Andersson, Z. G. Chen, V. D. Kulakovskii, A. Uddin, and J. T. Vallin, Phys. Rev. B **37**, 4032 (1988).
[68]T. G. Andersson, Z. G. Chen, V. D. Kulakovskii, A. Uddin, and J. Vallin, Appl. Phys. Lett. **51**, 752 (1987).
[69]M. Kudo and T. Mishima, Appl. Phys. **78**, 1685 (1995).
[70]D. Sun and E. Towe, Jpn. J. Appl. Phys. **33**, 702 (1994).
[71]T. S. Moise, L. J. Guido, J. C. Beggy, T. J. Cunningham, S. Seshardri, and R. C. Barker, J. Electron. Mater. **21**, 119 (1992).
[72]I. Sela, D. E. Watkins, B. K. Laurich, D. L. Smith, S. Subbanna, and H. Kroemer, Appl. Phys. Lett. **58**, 684 (1991).
[73]T. S. Moise, L. J. Guido, R. C. Barker, J. O. White, and A. R. Kost, Appl. Phys. Lett. **60**, 2637 (1992).
[74]K. Nishi and T. Anan, J. Appl. Phys. **70**, 5004 (1991).
[75]J. Cibert, R. André, C. Bodin, Le Si Dang, G. Feuillet, and P. H. Jouneau, Phys. Scr., T **49**, 487 (1993).
[76]D. Sun and E. Towe, Jpn. J. Appl. Phys. **33**, 702 (1994).
[77]S. Fafard, E. Fortin, and J. L. Merz, Phys. Rev. B **48**, 11062 (1993).
[78]A. N. Cartwright, D. S. McCallum, T. F. Boggess, A. L. Smirl, T. S. Moise, L. J. Guido, R. C. Barker, and B. S. Wherrett, J. Appl. Phys. **73**, 7767 (1993).
[79]X. R. Huang, D. R. Harken, A. N. Cartwright, D. S. McCallum, A. L. Smirl, J. L. Sánchez-Rojas, A. Sacedón, F. González-Sanz, E. Calleja, and E. Muñoz, J. Appl. Phys. **76**, 7870 (1995).
[80]D. Harken, X. R. Huang, D. S. McCallum, A. L. Smirl, J. L. Sánchez-Rojas, A. Sacedón, E. Calleja, and E. Muñoz, Appl. Phys. Lett. **66**, 857 (1995).
[81]J. L. Sanchez-Rojas, A. Sacedun, F. Calle, E. Calleja, and E. Munoz, Appl. Phys. Lett. **65**, 2214 (1994).
[82]T. E. Sale, J. Woodhead, G. J. Rees, R. Grey, J. P. R. David, A. S. Pabla, P. J. Rodriguez-Gíronés, P. N. Robson, R. A. Hogg, and M. S. Skolnick, J. Appl. Phys. **76**, 5447 (1994).
[83]M. Livingstone, I. Galbraith, and B. S. Wherrett, Appl. Phys. Lett. **65**, 2771 (1994).
[84]J. F. Valtuena, I. Izpura, J. L. Sanchez-Rojas, A. Sacedon, E. Calleja, and E. Munoz, Semicond. Sci. Technol. **10**, 1528 (1995).
[85]J. P. R. David, T. E. Sale, A. S. Pabla, P. J. Rodriquez-Gírones, J. Woodhead, R. Grey, G. J. Rees, P. N. Robson, M. S. Skolnick, and R. A. Hogg, Mater. Sci. Eng. B **35**, 42 (1995).
[86]Cooper, D. I. Westwood, and P. Blood, Appl. Phys. Lett. **69**, 2415 (1996).
[87]A. S. Pabla, J. Woodhead, E. A. Khoo, R. Grey, J. P. R. David, and G. J. Rees, Appl. Phys. Lett. **68**, 1595 (1996).
[88]P. O. Vaccaro, M. Hosoda, K. Fujita, and T. Watanabe, Jpn. J. Appl. Phys. **35**, 1292 (1996).
[89]O. Vaccaro, M. Takahashi, K. Fujita, and T. Watanabe, J. Cryst. Growth **150**, 503 (1995).
[90]Geoffrey Duggan, Karen J. Moore, Age Raukema, Gerke Th. Jaarsma, and Karl Woodbridge, Phys. Rev. B **45**, 4494 (1992).
[91]G. Arlt and P. Quadflieg, Phys. Status Solidi **25**, 323 (1968).
[92]K. Hübner, Phys. Status Solidi B **67**, 627 (1973).
[93]R. L. Tober and T. H. Bahder, Appl. Phys. Lett. **63**, 2369 (1993).
[94]T. B. Bahder, R. L. Tober, and J. D. Bruno, Phys. Rev. B **50**, 2731 (1994).
[95]D. Sun and E. Towe, Jpn. J. Appl. Phys. **33**, 702 (1994).
[96]H. Shen, M. Dutta, W. Chang, R. Moerkirk, D. M. Kim, K. W. Chung, P. P. Ruden, M. I. Nathan, and M. A. Stroscio, Appl. Phys. Lett. **60**, 2400 (1992).
[97]D. L. Smith, Solid State Commun. **57**, 919 (1986).
[98]R. A. Hogg, T. A. Fisher, A. R. K. Willcox, D. M. Whittaker, M. S. Skolnick, D. J. Mowbray, J. P. R. David, A. S. Pabla, G. J. Rees, R. Grey, J. Woodhead, J. L. Sanchez-Rojas, G. Hill, M. A. Pate, and P. N. Robson, Phys. Rev. B **48**, 8491 (1993).
[99]S. Cho, A. Sanz-Hervas, J. Kim, A. Majerfeld, and B. W. Kim, J. Appl. Phys. **96**, 1909 (2004).
[100]S. Cho, A. Majerfeld, A. Sanz-Hervas, J. J. Sanchez, J. L. Sanchez-Rojas, and I. Izpura, J. Appl. Phys. **90**, 915 (2001).
[101]J. J. Sanchez *et al.*, J. Appl. Phys. **91**, 3002 (2002).
[102]S. Cho, J. Kim, A. Sanz-Hervas, A. Majerfeld, G. Patriarche, and B. W. Kim, Phys. Status Solidi A **195**, 260 (2003).
[103]E. A. Caridi, T. Y. Chang, K. W. Goosen, and L. F. Eastman, Appl. Phys. Lett. **56**, 659 (1990).
[104]T. S. Moise, L. J. Guido, R. C. Barker, J. O. White, and A. R. Kost, Appl. Phys. Lett. **60**, 2637 (1992).
[105]P. Ballet, P. Disseix, J. Leymarie, A. Vasson, A-M. Vasson, and R. Grey, Phys. Rev. B **56**, 15202 (1997).
[106]C. Mailhiot and D. L. Smith, Phys. Rev. B **38**, 5520 (1988).
[107]O. Madelung (ed.), *Semiconductors* (Springer-Verlag, New York, 1982), Landolt-Börnstein, New Series, Vol 17.
[108]J. von Pezold, A. Dick, M. Friák, and J. Neugebauer, Phys. Rev. B **81**, 094203 (2010).
[109]O. Ambacher *et al.*, J. Phys. Condens. Matter **14**, 3399 (2002).
[110]P. Ballet, P. Disseix, J. Leymarie, A. Vasson, A.-M. Vasson, and R. Grey, Phys. Rev. B **59**, R5308 (1999).
[111]K. Yang, T. Anan, and L. J. Schowalter, Appl. Phys. Lett. **65**, 2789 (1994).